

Review: MR Physics for Clinicians**Body MRI Artifacts in Clinical Practice: A Physicist's and Radiologist's Perspective****CME**Martin J. Graves, PhD,^{1*} and Donald G. Mitchell, MD²

This article is accredited as a journal-based CME activity. If you wish to receive credit for this activity, please refer to the website: www.wileyhealthlearning.com

ACCREDITATION AND DESIGNATION STATEMENT

Blackwell Futura Media Services designates this journal-based CME activity for a maximum of 1 *AMA PRA Category 1 Credit*[™]. Physicians should only claim credit commensurate with the extent of their participation in the activity.

Blackwell Futura Media Services is accredited by the Accreditation Council for Continuing Medical Education to provide continuing medical education for physicians.

EDUCATIONAL OBJECTIVES

Describe the causes and cures of a variety of artifacts encountered in body MRI.

ACTIVITY DISCLOSURES

No commercial support has been accepted related to the development or publication of this activity.

Faculty Disclosures:

Editor-in-Chief: Mark E. Schweitzer, MD, discloses DSMB work for Paradigm Spine, and consultation for MMI.

CME Editor: Scott B. Reeder, MD, PhD has no conflicts of interest to disclose.

CME Committee: Pratik Mukherjee, MD, PhD, Shreyas Vasanawala, MD, PhD, Bonnie Joe, MD, PhD, Tim Leiner, MD, PhD, Sabine Weckbach, MD, and Frank Korosec, PhD have no conflicts of interest to disclose. Scott K. Nagle, MD, PhD discloses a personal shareholder investment in GE. Mustafa R. Bashir, MD discloses research support from Bracco Diagnostics and Siemens Healthcare, and consultant honorarium from Bayer Pharmaceuticals.

Authors: Martin J. Graves, PhD, and Donald G. Mitchell, MD has no conflicts of interest to disclose.

This manuscript underwent peer review in line with the standards of editorial integrity and publication ethics maintained by *Journal of Magnetic Resonance Imaging*. The peer reviewers have no relevant financial relationships. The peer review process for *Journal of Magnetic Resonance Imaging* is double-blinded. As such, the identities of the reviewers are not disclosed in line with the standard accepted practices of medical journal peer review.

Conflicts of interest have been identified and resolved in accordance with Blackwell Futura Media Services's Policy on Activity Disclosure and Conflict of Interest. No relevant financial relationships exist for any individual in control of the content and therefore there were no conflicts to resolve.

INSTRUCTIONS ON RECEIVING CREDIT

For information on applicability and acceptance of CME credit for this activity, please consult your professional licensing board.

This activity is designed to be completed within an hour; physicians should claim only those credits that reflect the time actually spent in the activity. To successfully earn credit, participants must complete the activity during the valid credit period.

Follow these steps to earn credit:

- Log on to www.wileyhealthlearning.com
- Read the target audience, educational objectives, and activity disclosures.
- Read the article in print or online format.
- Reflect on the article.
- Access the CME Exam, and choose the best answer to each question.
- Complete the required evaluation component of the activity.

This activity will be available for CME credit for twelve months following its publication date. At that time, it will be reviewed and potentially updated and extended for an additional period.

¹Department of Radiology, Cambridge University Hospitals, Cambridge, United Kingdom.

²Department of Radiology, Thomas Jefferson University, Philadelphia, Pennsylvania, USA.

*Address reprint requests to: M.J.G., MRIS Unit, Box 162, Cambridge University Hospitals NHS Foundation Trust, Hills Road, Cambridge, CB2 0QQ UK. E-mail: mjg40@cam.ac.uk

Received October 24, 2012; Accepted May 24, 2013.

DOI 10.1002/jmri.24288

View this article online at wileyonlinelibrary.com.

The high information content of MRI exams brings with it unintended effects, which we call artifacts. The purpose of this review is to promote understanding of these artifacts, so they can be prevented or properly interpreted to optimize diagnostic effectiveness. We begin by addressing static magnetic field uniformity, which is essential for many techniques, such as fat saturation. Eddy currents, resulting from imperfect gradient pulses, are especially problematic for new techniques that depend on high performance gradient switching. Nonuniformity of the transmit radiofrequency system constitutes another source of artifacts, which are increasingly important as magnetic field strength increases. Defects in the receive portion of the radiofrequency system have become a more complex source of problems as the number of radiofrequency coils, and the sophistication of the analysis of their received signals, has increased. Unwanted signals and noise spikes have many causes, often manifesting as zipper or banding artifacts. These image alterations become particularly severe and complex when they are combined with aliasing effects. Aliasing is one of several phenomena addressed in our final section, on artifacts that derive from encoding the MR signals to produce images, also including those related to parallel imaging, chemical shift, motion, and image subtraction.

Key Words: MRI, artifacts, body imaging, image quality
J. Magn. Reson. Imaging 2013;38:269–287.
 © 2013 Wiley Periodicals, Inc.

MRI IS UNDOUBTEDLY the most powerful and versatile diagnostic imaging method ever created. With this power, however, comes complexity, and some features in an image may be unintended, unexpected and poorly understood. We generally refer to these features as artifacts, because they may lead to interpretive difficulties or errors. The best remedy for MRI artifacts and their potential to produce diagnostic errors is to promote understanding, so that they can be prevented or, alternatively, one can use the information content of an artifact to contribute to diagnostic content.

Because artifacts can arise from either the MR system hardware alone or through the interaction of the patient with the hardware we have chosen to present the artifacts, first, through effects due to the static magnetic field, gradients, and radiofrequency system, before addressing artifacts related to the encoding of the MR signals. We have primarily concentrated on artifacts relevant to body MRI and acknowledge that we have not provided a comprehensive review of all MRI artifacts. The interested reader is, therefore, directed to other review articles in the literature (1–6).

B₀ ARTIFACTS

Static magnetic field (B₀) uniformity is required for all MR imaging. Manufacturing tolerances and the local installation environment means that the main magnetic field needs to be optimized at installation by the manufacturer who “shims” the magnet either passively, using small pieces of metal distributed around

the room temperature bore of the magnet, or actively by adjusting the currents through additional superconducting coils within the magnet cryostat.

Magnetic field uniformity is usually reported as the root mean square (rms) variation from the nominal field strength, e.g., 3.0 tesla (T), in either parts-per-million (ppm), or as a frequency variation in Hz, over a large number of points within a given diameter spherical volume (DSV). A typical 3.0T manufacturer’s shim would have an rms value of 50 Hz or 0.4 ppm over a 45 cm DSV. Because heterogeneous susceptibility within the human body will affect local magnetic field uniformity, manufacturers also provide methods of patient specific shimming. This involves rapidly mapping the static magnetic field uniformity, usually using a gradient echo-based phase difference technique, and adjusting the offsets on the x, y, and z gradients to remove any linear field variations (7). Some systems may be equipped with additional room-temperature, i.e., nonsuperconducting, higher order shim coils that can further improve the uniformity, particularly over small volumes.

Chemical Shift Selective Fat Saturation

Uniformity of B₀ is important for chemical shift selective fat saturation techniques. Human adipose tissue is composed primarily of triglycerides, which are a subgroup of lipid molecules. Triglycerides comprise multiple groups of protons (CH₃, CH₂, CH=CH etc), with the nuclear shielding effect resulting in a range of chemical shifts from 0.9 to 5.3 ppm lower than the water (H₂O) proton resonance. The most abundant triglyceride resonance comes from the methylene (CH₂) groups, in which the protons resonate at approximately 3.4 ppm lower than those in water. Hence at 1.5T the methylene peak appears at 3.4 ppm * 64 MHz = 220 Hz lower than the water resonant frequency. Chemical shift selective saturation pulses at 1.5T are, therefore, centered around –220 Hz from water. These pulses have a bandwidth that is sufficiently narrow so as to avoid saturating the water signal. A typical 1.5T chemical shift saturation pulse has a bandwidth of approximately 150 Hz. Therefore, to obtain good fat saturation it is necessary that the main magnetic field not vary by more than 150 Hz across the entire field-of-view and across all slices in a multislice acquisition. If this is not the case, the fat saturation will be suboptimal.

Magnetic field nonuniformity due to patient susceptibility is particularly problematic at air tissue interfaces, which are especially abundant in various locations within the chest, including the breast (Fig. 1). Failure of fat saturation is almost inevitable when the air tissue interface is oriented along the z-axis of the magnetic field (8–10). One particularly common example is adipose tissue situated anterior to the liver, immediately inferior to the lung base (Fig. 2). Heterogeneous susceptibility within the patient can also cause the water frequency to be shifted so that it falls within the bandwidth of the fat saturation pulse. In this situation, the water signal can also become saturated. This effect has

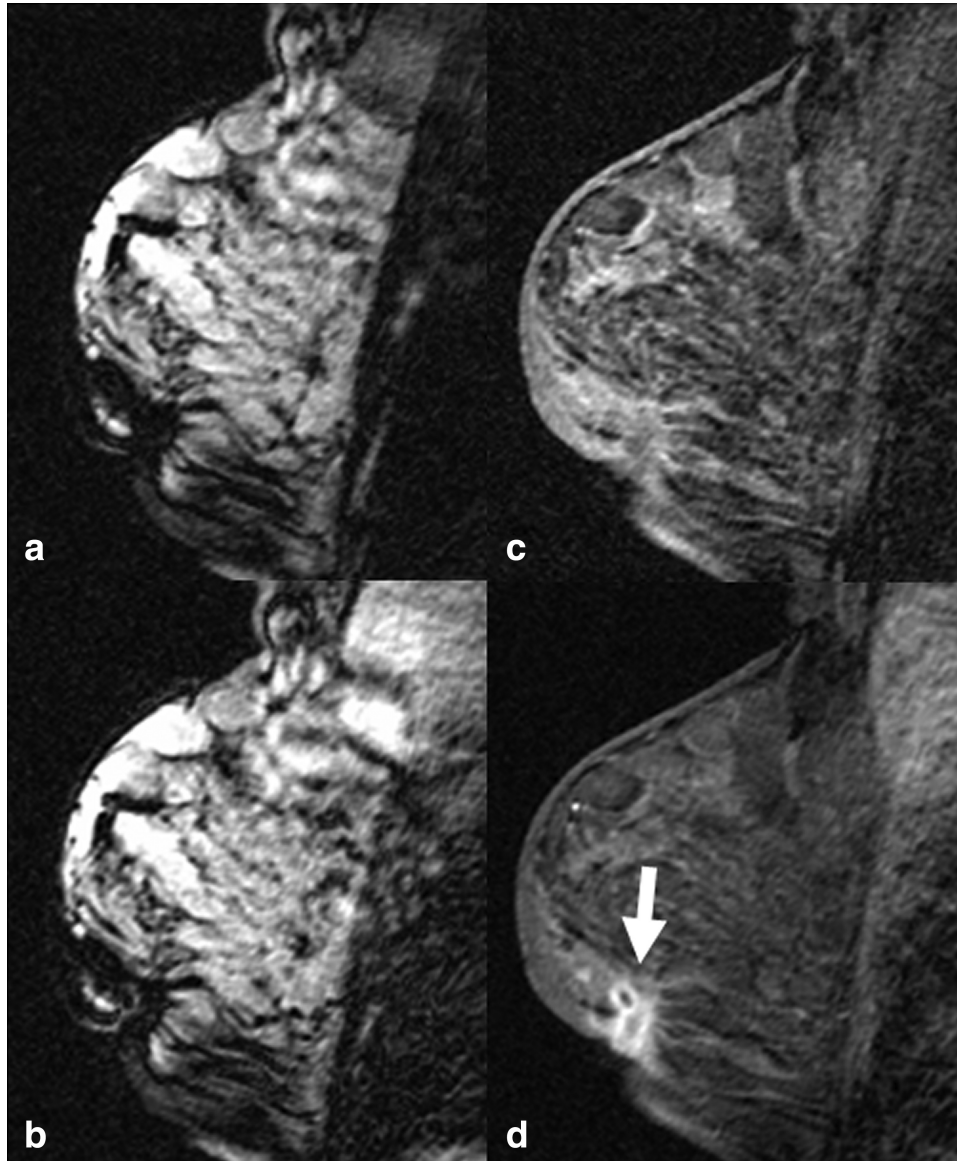


Figure 1. Examples of poor fat saturation in the breast due to susceptibility differences caused by patient anatomy. **a:** Sagittal T1-weighted 3D GRE image of the breast, with unsuccessful fat saturation. Nonfatty tissue has low signal intensity. **b:** As in **a** but after contrast agent injection. There is no enhancing tissue. **c:** Sagittal image of the breast, repeated 1 week after **a** and **b**, with better fat saturation. **d:** As in **c** but after contrast agent injection. Arrow indicates enhancement of recurrent breast carcinoma.

also been reported in contrast-enhanced thoracic angiography (11).

Blood flow along the long axis of the magnet can further compound artifacts related to suboptimal fat saturation, most typically affecting rapidly flowing blood within the thoracic or abdominal aorta. Because this fat saturation pulse is not spatially selective, the frequency of water above the imaging volume may be lower so that it matches the frequency of the fat saturation pulse. The saturated water in the aorta may then flow inferiorly into the region of interest, and appear suppressed on the resulting image (Fig. 3). Because of this interaction between magnetic field nonuniformity and blood flow, signal in the aorta is commonly suppressed even if fat saturation otherwise appears optimal elsewhere in a given image. For this

reason, fat saturation should be used with caution with bright-blood imaging of the aorta.

Water/Fat Separation

Because water and fat precess at different frequencies, their relative signal phases will vary as a function of echo time in a gradient echo sequence. At 1.5T, a echo time (TE) of $1/220 \text{ Hz} = 4.6 \text{ ms}$ will mean that the signals from water and fat will be in-phase (IP), whereas at half this value, i.e., $\text{TE} = 2.3 \text{ ms}$, they will be in opposed-phase (OP) (see “Chemical Shift Effects” below). Two-point Dixon techniques of fat suppression (12), often referred to as fat separation, involve calculating images consisting of water or fat only from IP and OP images. Two-point Dixon fat

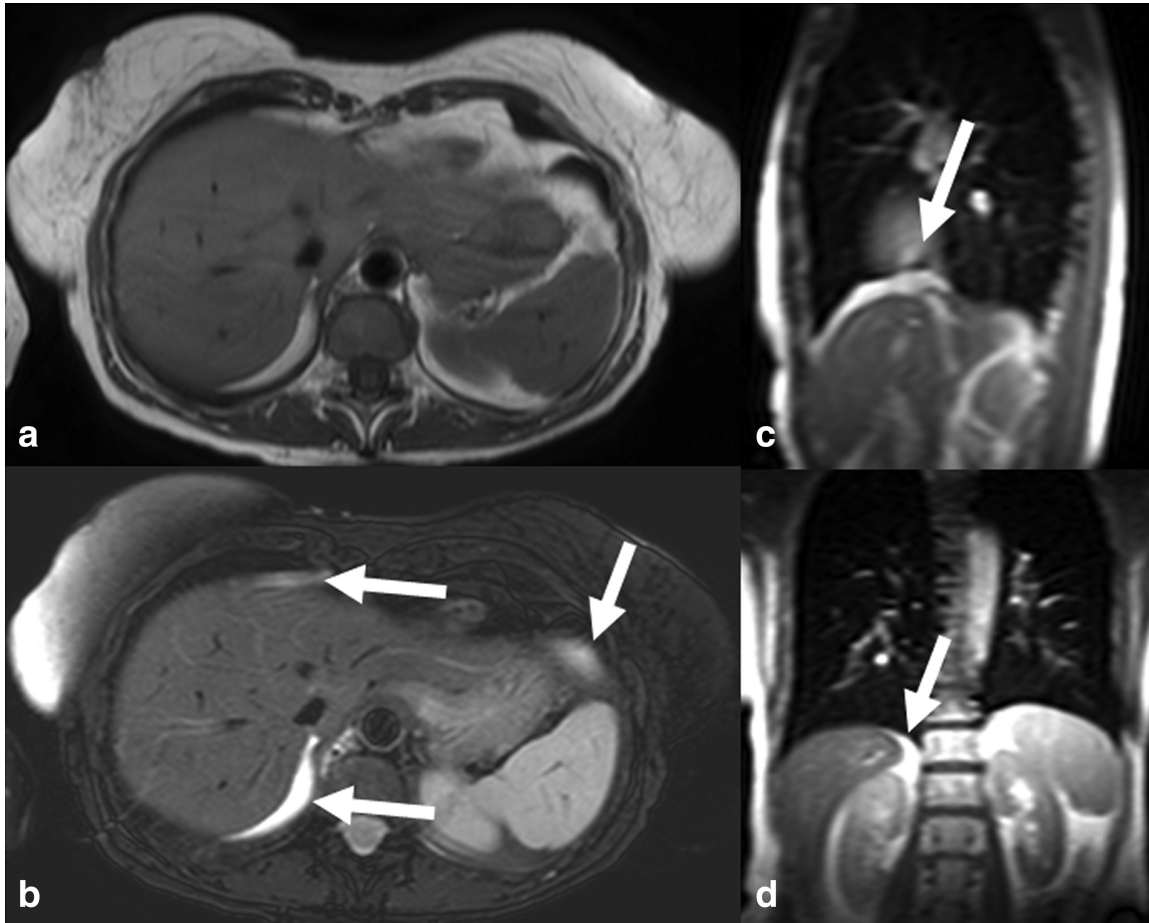


Figure 2. Example of poor fat saturation near the liver due to air-tissue susceptibility differences. **a:** Axial T1-weighted image of the superior portion of the liver. Note the adipose tissue at the edges of the liver. **b:** Axial fat suppressed T2-weighted image at same location. Although most of the intra-abdominal adipose tissue is saturated, the adipose tissue adjacent to the liver is not saturated (arrows). Sagittal (**c**) and coronal (**d**) T1-weighted images show the adipose tissue (arrow) directly inferior to the lungs. The air-tissue susceptibility difference has caused the fat saturation failure.

separation techniques were initially available mainly on low field, e.g., 0.3T, MRI systems, where fat saturation is particularly difficult due to the smaller chemical shift between water and methylene protons; the shift is proportional to the magnetic field strength, so it is only one fifth the magnitude compared with 1.5 T, i.e., 44 Hz rather than 220 Hz.

In recent years two-point Dixon fat separation techniques have become commercially available alternatives to fat saturation at 1.5T and 3T. However, they are also sensitive to B_0 variations and require sophisticated postprocessing algorithms to ensure that each voxel is correctly assigned as either water or fat (13). Although these algorithms are generally quite robust, they can fail in regions of high field nonuniformity. Figure 4 shows a water only image from a three-dimensional (3D) two-point Dixon acquisition demonstrating uncorrected fat swaps in the corners of the image. In the presence of such regions, alternative three-point techniques such as iterative decomposition of water and fat with echo asymmetric and least-squares estimation (IDEAL) (14) can improve fat suppression because the acquisition method uses images with three separate echo times to calculate a

B_0 field map as part of the reconstruction process. This field map helps to correctly categorize each pixel as either water or fat, allowing a more robust correction for susceptibility differences and other causes of magnetic field nonuniformity.

Failure of fat saturation can result not only from B_0 nonuniformity, but also from poor transmit field (B_1^+) uniformity (see “Receive Field” below), particularly at 3T and higher. The use of adiabatic pulses that have improved B_1^+ uniformity have also been found to improve fat saturation (15).

Balanced Steady State Free Precession

Fully rewound gradient echo sequences, known generically as balanced steady-state-free-precession (bSSFP) (16) but also by vendor-specific terms such as True-FISP (Siemens), b-FFE (Philips) and FIESTA (GE), are also sensitive to B_0 nonuniformity. The sensitivity of the bSSFP sequence to field nonuniformity results in spectral “notches” at specific frequency offsets that can result in banding artifacts where there is a rapid phase transition between 0 and π in the bSSFP signal (17). The phase of the bSSFP signal alternates between 0

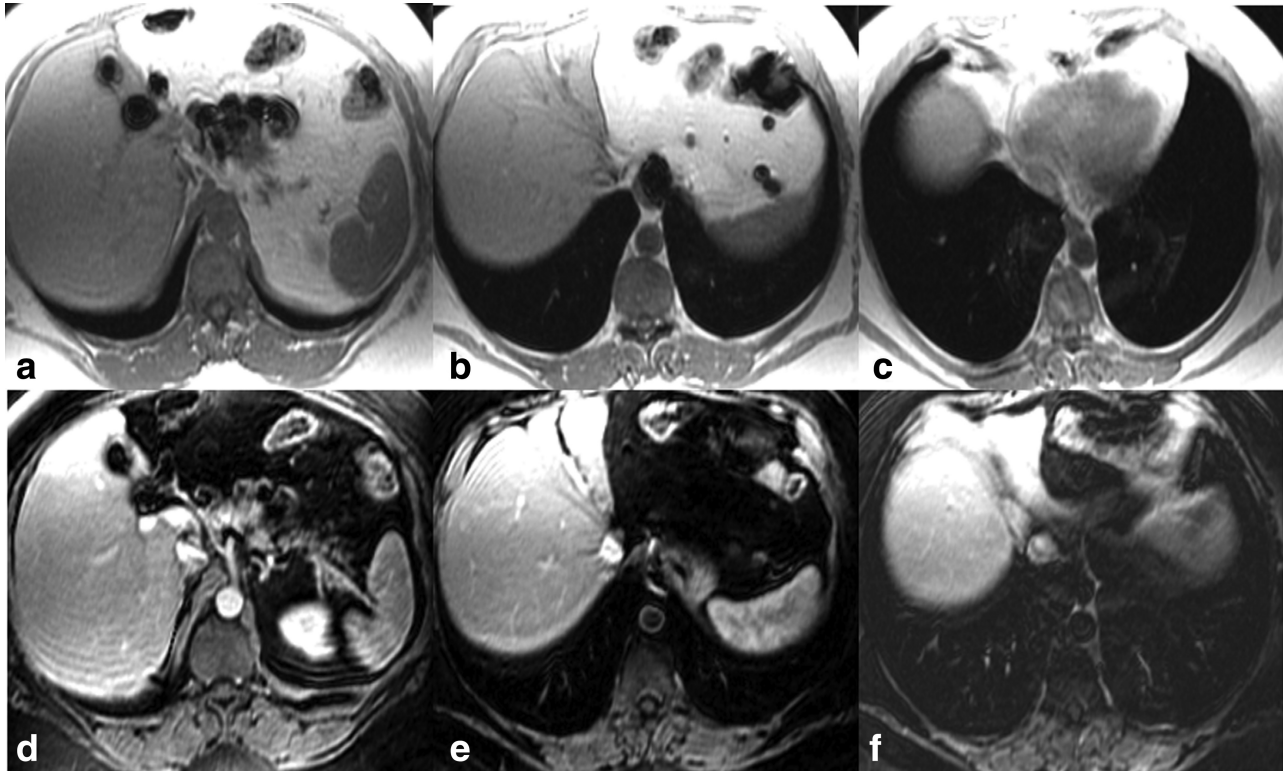


Figure 3. Aortic lumen signal loss due to fat saturation. a–c: Show T1-weighted images without fat saturation. d: The 3D gradient echo T1-weighted image with fat saturation, at level corresponding to a. The aorta and other vessels show enhancement, shortly after injection of contrast agent. e: Same acquisition but at a location superior to d. Note that the wall of the aorta is enhanced, but signal in the aortic lumen is saturated, while the other vessels are enhanced. The fat signal is saturated, including fat surrounding the aorta. f: Image superior to e. Fat saturation is poor, and water suppression has obscured enhancement of the aortic wall. Saturation of the inferiorly flowing blood in the aorta accounts for the signal void in the aortic lumen in e. The saturated blood has not extended inferiorly enough to decrease the intensity of the aortic lumen in d.

and π for every $\pm 2\pi$ of off-resonance phase developed during one TR period. Figure 5 shows an example where the TR is 3.8 ms, and, therefore, a π phase change occurs at $\pm 1/(2 \times 3.8\text{ms}) = \pm 131.5\text{Hz}$ which

appears as a black band artifact. Banding artifacts can, therefore, be reduced by using the shortest possible TR, and by improving the magnetic field uniformity through shimming.

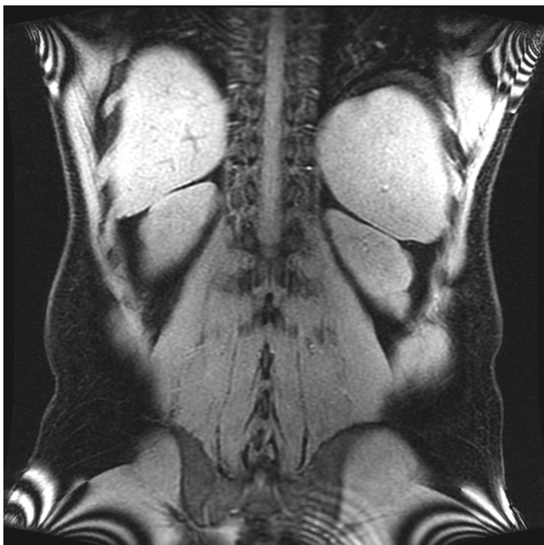


Figure 4. A two-point Dixon technique showing the water only image. Note the fat swaps in the corners of the image where B_0 and the gradient field are nonuniform.

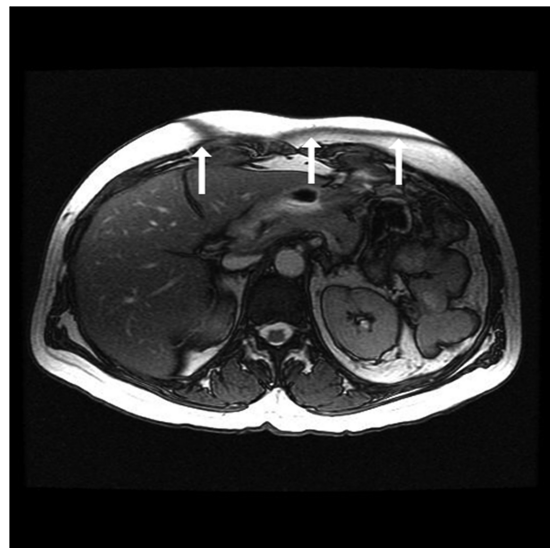


Figure 5. Balanced steady state free precession image acquired with a TR of 3.8 ms. Note the anterior banding artifact (arrows) where the frequency offset due to B_0 nonuniformity is 131.5 Hz.

Metal

Artifacts related to metal can be minimized by using techniques that are less dependent on high magnetic field uniformity. Spin echo or fast spin echo techniques are less degraded by susceptibility artifact. If a gradient echo technique must be used, minimizing the TE can reduce the size of the resulting signal void near the metallic object, as well as any other artifact from susceptibility. Increasing the sampling (receiver) bandwidth can also reduce the severity of susceptibility artifact, because this increases the magnitude of the frequency differences related to the imaging gradients relative to those due to the metallic object (18). One important method to reduce artifact from metal is to avoid the use of fat saturation.

GRADIENT ARTIFACTS

Eddy Currents

Because the gradient coils are positioned inside the room temperature bore of the magnet, switching of the gradient pulses in an MRI pulse sequence induces currents in the conducting structure of the magnet cryostat. These currents, known as “eddy-currents,” create their own magnetic fields that distort the gradient waveforms, causing a variety of artifacts depending upon the pulse sequence. Manufacturers work hard to reduce the effects of eddy currents, but this is challenging because higher performance gradients tend to induce greater eddy currents, and many new sophisticated imaging sequences are more sensitive to eddy current induced gradient distortions.

There are two main approaches to reducing eddy currents. The first involves the use of actively or self-shielded gradient coils in which the primary gradient coil is surrounded by a secondary, sometimes referred to as a shield set of coils, at a larger radius (19,20). The direction of the current in the secondary coils is opposite to that of the primary coil, so that the gradient fields nearly cancel each other at the larger radius of the magnet cryostat. Hence, the eddy current inducing fields are substantially reduced. It is necessary for the primary and secondary coils to have a sufficiently large radius ratio so that the field from the secondary coil does not cancel too much of the desired gradient field from the primary coil within the imaging volume.

The second approach to minimize eddy currents, which was the only solution before the development of actively-shielded gradients, is to use pre-emphasis (21,22). This is a method whereby the gradient pulses are deliberately distorted so that when combined with the fields created by the eddy currents the net resultant is the desired gradient waveform. As part of the initial MRI system tuning, the installation engineer measures the magnetic fields created by the eddy currents to determine how the gradient pulses should be distorted, a process known as eddy-current calibration or compensation. Unfortunately, the eddy currents created in the cryostat can be very complex

and it is not possible, even with actively shielded gradient coils and pre-emphasis, to completely cancel the eddy current fields.

Because the residual eddy currents result from gradient pulses, any changes in gradient pulses, such as varying the strength of the phase encoding gradient from TR to TR, can lead to signal instabilities and hence image artifacts. Large motion encoding gradients such as those used in diffusion-weighted imaging or phase-contrast velocity mapping can suffer from eddy current-induced artifacts (23,24). Fast, or turbo, spin echo imaging sequences can also demonstrate ghosting artifacts due to the effects of eddy currents, as well as other instabilities, causing undesired phase shifts in the echo signals. Various phase correction algorithms have been proposed that attempt to correct these artifacts (25,26).

Gradient Nonlinearity

A limitation of all MRI systems is that the magnetic fields produced by the gradient coils are nonlinear, particularly at the edges of large fields-of-view. This nonlinearity is due to design trade-offs required to achieve the desired system performance. However, the system manufacturer knows how the gradient coils are designed and can, therefore, correct for these nonlinearities by “warping” the reconstructed images (27). Figures 6a and b show the effect of gradient nonlinearity on coronal images obtained in a regular grid phantom and in vivo with a 48 cm field-of-view. Figures 6c and d show the effect of a software gradient nonlinearity correction applied after image reconstruction. Unfortunately, these correction schemes are not completely effective in removing these distortions. While this may not have a significant impact on image review it may be important for accurate quantitative measurements and for precise MR-guided intervention or radiotherapy planning (28). It should also be noted that these correction algorithms not only spatially remap the pixel data but also involve an apparent change in pixel intensity in the warped regions (28). This may affect the accuracy of calculations that involve measuring signal intensities in these regions.

RADIOFREQUENCY ARTIFACTS

Transmit Field

The objective of the radiofrequency (RF) transmit system is to create a uniform time-varying magnetic field to tip the net magnetization. This magnetic field is usually referred to as B_1 , and is applied perpendicular to the static magnetic field B_0 . Because RF coils are used to transmit and receive B_1 , the fields are often annotated with a + or - superscript to indicate transmit and receive respectively.

The system body coil is usually used to generate B_1^+ because this coil has a large diameter and, therefore, can produce the most uniform transmit field, i.e., ideally a uniform flip angle across the subject. At 3T, and to a lesser extent at 1.5T, B_1^+ nonuniformity artifacts are common. These artifacts, appearing as

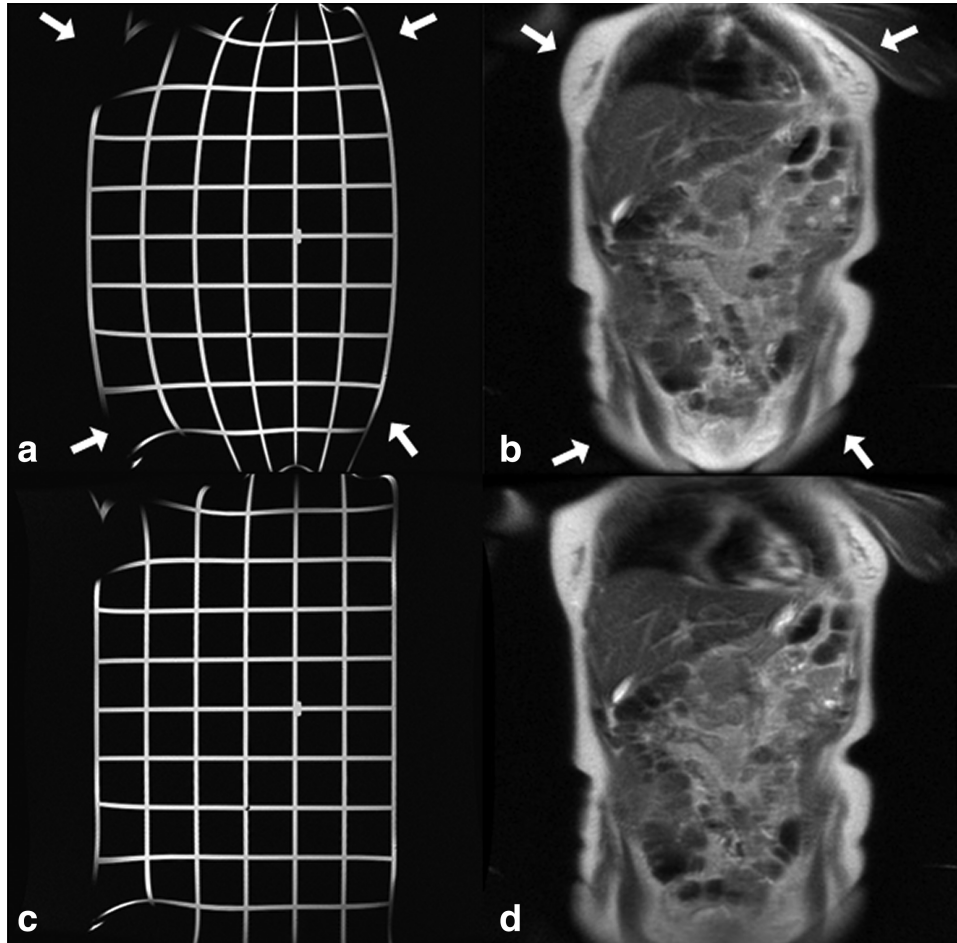


Figure 6. Gradient nonlinearity artifact and correction. **a:** A coronal image of a regular grid phantom acquired with a 48 cm field-of-view. The arrows point to regions of gradient nonlinearity. **b:** A coronal in vivo fast spin echo image without gradient nonlinearity correction. The arrows point to regions of nonlinearity. **c,d:** Show the same phantom and in vivo images but after software gradient nonlinearity correction.

regions with increased or decreased signal, are caused by constructive or destructive interference between RF standing waves (29). The problem is more severe at higher field strengths because the wavelength of the RF wave decreases as the frequency of B_0 increases.

The wavelength λ of the RF wave is given by:

$$\lambda = \frac{c}{f_0 \cdot \sqrt{\epsilon}} \quad [1]$$

Where c is the speed of light ($c = 3 \times 10^8 \text{ ms}^{-1}$), f_0 is the Larmor frequency and ϵ is the dimensionless dielectric (or static relative permittivity) constant of water ($\epsilon = 81$). At 1.5T ($f_0 = 63.9 \times 10^6 \text{ Hz}$) this results in a wavelength of 52 cm, which is larger than the girth of most subjects. However, at 3T ($f_0 = 127.8 \times 10^6 \text{ Hz}$) the wavelength becomes 26 cm. This is of the same order as the girth of the subject and in body imaging can often result in destructive interferences of the transmitted wave resulting in regional hypointensities (Fig. 7a).

One method used to reduce the signal nonuniformity is to position a dielectric or RF cushion/pad anteriorly and sometimes posteriorly on the body in an attempt to passively change the geometry of the B_1^+ field

distribution and hence change the phase of the RF standing waves (30,31) thereby reducing or eliminating the nonuniformity. The pad contains a low conductivity material with a high dielectric constant, typically $\epsilon > 50$ together with an appropriate doping agent such that the pad does not appear in the MR images.

Ascites, or other fluid collections within the abdomen, can also give rise to a similar nonuniformity artifact. However, in this case, the shading is due to the RF waves creating eddy currents within the fluid that in turn create their own magnetic fields that oppose the RF waves. These fields attenuate the RF waves thereby causing regional signal hypointensities (32).

More recently, particularly with the development of wide bore MRI scanners (patient aperture diameter $\geq 70 \text{ cm}$), manufacturers have implemented a method known as B_1^+ -shimming, where the two quadrature ports of the body coil are independently driven (33). A standard body coil is of a birdcage design, which has two connections to the RF amplifier that are physically 90° apart on the coil. These two body coil ports are driven by the RF amplifier through a "quad-hybrid," which splits the power into two quadrature, i.e., 90° apart, signals achieving a circularly polarized

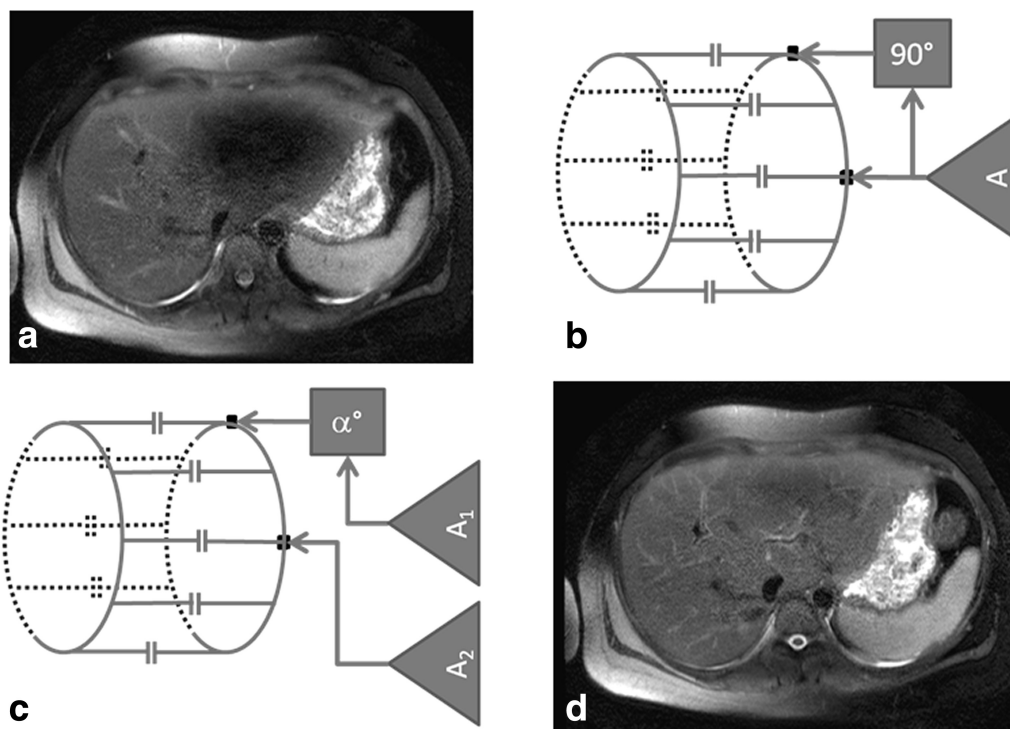


Figure 7. B₁⁺ shimming. **a:** Shows central signal shading due to standing wave artifact observed with a standard single transmitter wide-bore 3.0T system. **b:** Shows a standard transmitter arrangement with a single amplifier (A) and a 90° phase shift between the two ports of the birdcage transmit coil. **c:** Dual transmit arrangement with two amplifiers (A₁ and A₂) allowing independent control of the waveform amplitude and a variable phase shift α° between the two ports of the birdcage coil. **d:** The standing wave artifact is reduced using a dual transmit system.

B₁⁺ excitation (Fig. 7b). Circular polarization is highly advantageous because all of the RF power is coupled to the natural direction of nuclear precession. In the case of standing waves, however, circular polarization may not be optimal. Various approaches to B₁⁺-shimming adopted by the manufacturers range from setting a fixed, but nonorthogonal, i.e., $\neq 90^\circ$, phase shift between the two channels, to driving each channel independently by two separate RF amplifiers, thereby controlling both the phase and amplitude of the RF signal applied to each port (Fig. 7c). It is difficult to decide exactly what phase shift, and possibly relative amplitudes, are required. Some manufacturers use single fixed values, whereas others have derived look-up tables whereby the “optimal” parameters are established on the basis of an individual subject’s height, weight and body area to be scanned. Finally some vendors have implemented B₁⁺-mapping techniques that optimize the parameters on a per subject and per region basis, analogous to the patient specific auto-shimming methods that are currently used to optimize B₀ uniformity (34,35). Figure 7d shows the effect of a dual transmit system in reducing standing wave artifacts in a wide-bore 3.0T system.

Receive Field

Whereas birdcage coils have high transmission and reception uniformity, their design does not necessarily lead to the best image signal-to-noise ratio (SNR).

SNR is optimized by using coils with a small diameter, although this leads to problems with coverage and depth penetration. These conflicting characteristics of small coils led to the development of coil arrays whereby several small coils are arranged together to achieve the necessary coverage but with the SNR advantage of having small individual coils (36). Each coil is connected to its own RF receiver chain and the final image is a combination of the individual images from each coil. However, unlike birdcage coils, this causes image intensity to vary with depth, particularly for arrays that encompass a large volume of tissue. Manufacturers offer several methods to mitigate this effect (37), which usually involve taking the ratio of a low resolution image obtained with the coil array and the same low resolution image obtained using the body coil. This allows calculation of a smoothly varying coil sensitivity correction map, which is applied to the array images. It is important to note that an intensity correction algorithm such as this does not compensate for lower SNR in the center of a large body part. This usually manifests as a grainy appearance of the low SNR zone, even if the displayed intensity is adequately corrected.

In addition to the inherent spatial sensitivity of coil arrays, there are occasions when individual coil elements may fail, also causing a shading artifact. Figure 8a shows an image from a 4 channel array coil where the coil in the bottom right corner (arrowed) has failed. Figure 8b shows the same image but with all coil elements working correctly. In this example the

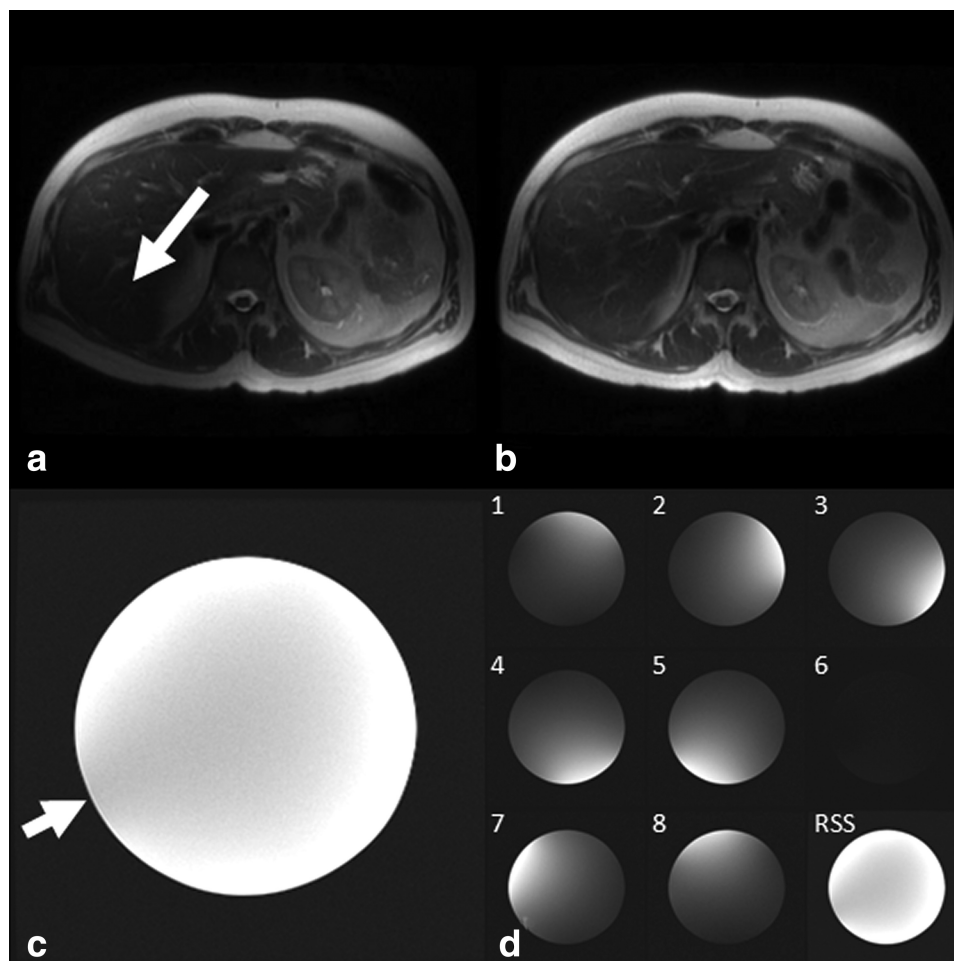


Figure 8. RF coil element failure. **a:** 4-channel combined array coil image but with a failure of one coil element in the bottom left hand corner (arrow). **b:** combined array coil image with all individual coil elements working correctly. **c:** combined image from an 8-channel volume coil demonstrating a subtle signal hypointensity (arrow). **d:** saving the individual coil images clearly shows a failure of coil element 6 consistent with the region of signal hypointensity in **c**. RSS is the root-sum-of-squares reconstruction that combines all 8 images.

shading is obvious, but with a higher number of coil elements in the array, the shading from one failed coil may be subtle.

One method to confirm a faulty coil is to reconstruct the images from each individual coil element. Figure 8c shows an image of a uniform phantom acquired using an eight-channel volume coil with one failed coil element. This manifests in the combined image as a subtle signal hypointensity. Reconstruction of images from each of the individual coils, however (Fig. 8d), clearly shows absent signal from coil 6 the position of which is consistent with the artifact seen in Figure 8c. Reviewing the signal from all elements is an important part of a regular coil quality assurance program, as simply checking the overall SNR of the combined coil may not be sensitive enough to detect such a failure.

Fast Spin Echo Cusp Artifacts

Artifacts due to peripheral signals, i.e., arising from outside the imaging volume, are sometimes seen in fast spin echo (FSE) images acquired in the sagittal or

coronal plane with the phase-encoding direction superior-inferior. The artifact has previously been described as a dot or a “C”-shaped signal region leading to it being called a “cusp” artifact (38). The artifact is due to the RF excitation, and the subsequent detection of signal, from tissue that is outside the linear region of the magnetic field gradients. Gradient nonlinearity, combined with B_0 nonuniformity, toward the end of the gradient coil, results in the tissue experiencing the same magnetic field as at isocenter (39) (Fig. 9a). This point of equal magnetic field, in the superior-inferior direction away from isocenter, is known as the “gradient null” and effectively provides no spatial localization. If an RF array coil element is active in this region the received signal may alias (see “Phase Aliasing” below), into the imaging volume as a cusp artifact. Alternatively, even if the signal does not directly alias into the imaging volume, system instabilities such as eddy currents or intrinsic FSE signal modulations may cause ghosting of the signal into the imaging volume (40). The bright spot, or star-like, artifact is sometimes referred to as “startifact,” whereas the ghosting or ribbon-like artifact is sometimes

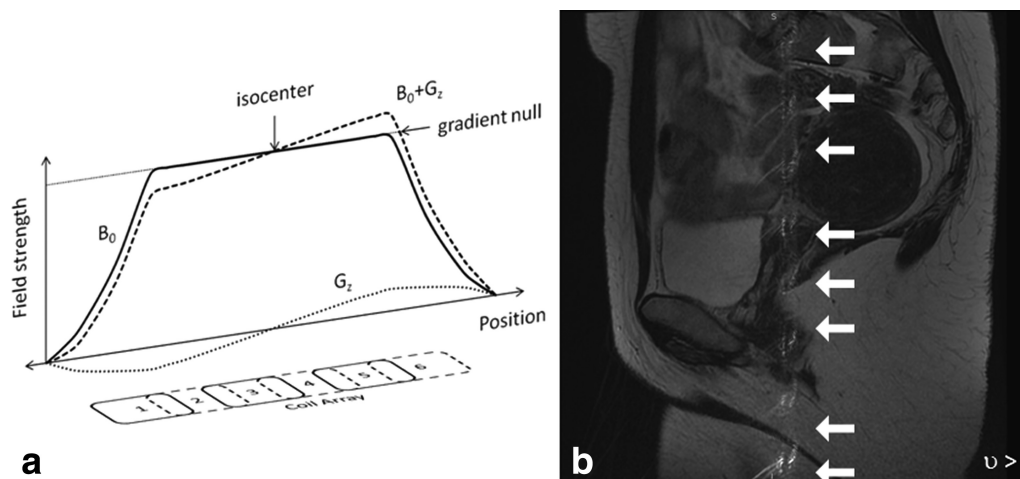


Figure 9. Peripheral signal artifact. **a:** The summation of gradient (G_z) and B_0 nonuniformity give rise to a gradient null. If tissue is present at this position it will have the same frequency as at isocenter. Any active coil in this region will receive the signal and if the phase encoding direction is in this direction then the signal will alias into the imaging volume. Depending upon the signal evolution and any system instabilities the artifact will appear differently, e.g., as a point, star or ribbon. **b:** Shows a ribbon-type peripheral signal artifact (arrows) in a coronal fast spin echo acquisition with the phase encoding direction oriented superior-inferior. The v shows the frequency encoding direction.

referred to as “annefact” (41). Figure 9b shows a ribbon-like artifact in a sagittal spine image where the phase encoding direction is aligned along the superior-inferior (SI) direction of the patient to minimize artifacts from respiration in the anterior-posterior direction. Usually no-phase-wrap techniques are used to avoid tissue signal outside the prescribed field of view (FOV) from being aliased into the image, however, they are not effective in eliminating peripheral signal artifacts. A simple solution to avoiding these artifacts is to match the receiver coils to the desired FOV so that there are no active coils outside the FOV of interest to detect these unwanted peripheral signals, ensuring that they do not get aliased into the final image (41).

Radiofrequency Interference

Many image artifacts result from undesired RF signals that corrupt the MR data. This undesired RF may arise externally or internally to the MR system. External sources are usually minimized by locating the magnet inside an RF shielded enclosure or cabin. This cabin provides a high degree of immunity from external interference, and prevents leakage of the high power RF from the MR system. However, if there is a problem with this enclosure then external RF can enter the MR receiver system. If this interference is periodic with either single or multiple frequencies then the artifact typically appears as a bright and dark alternating pattern in the phase encoding direction that is often referred to as a zipper artifact.

The periodic RF interference described above should be contrasted with short intense artifacts that affect only single points in k -space, called spike-noise or white pixel noise (42). One or more spikes of detected external noise may produce a patterned degradation of the image. Depending upon where this point occurs in k -space the overall image, after Fourier transformation, will demonstrate a superimposed

banding artifact corresponding to that spatial frequency. A spike occurring near the centre of k -space will have a low frequency banding, whereas a spike occurring near the edge of k -space will generate a high frequency banding. This cross-hatching appearance is sometimes referred to as a “corduroy” (single spike) or “herringbone” (multiple spikes) artifact. Causes of such artifact can include static electricity from clothing or blankets, or random noise from electrical sources such as damaged filament light bulbs. Figure 10 shows several examples of severe degradation due to static electricity from an acrylic sweater, which resolved following removal of the subject’s sweater.

MR ENCODING ARTIFACTS

Phase Aliasing

MRI allows different FOVs to be selected in the frequency and phase encoding direction. In the frequency encoding direction the FOV and the readout (receiver) bandwidth are selected by the operator. These two pieces of information allow the system to calculate the desired frequency encoding gradient strength. The readout bandwidth information is also used by the system to electronically filter out any frequencies outside of the bandwidth. However, in the phase encoding direction, the signal encoding is achieved through the phase imparted to the spins (43), so there is no direct equivalent to electronic filtering in the frequency encoding direction. The desired phase FOV can also be chosen by the operator but in this case any tissue that exists outside this FOV will be encoded incorrectly. The phase encoding gradient amplitudes are calculated so as to achieve a maximum 360° phase shift across the selected FOV. This means that any tissue beyond the FOV will be phase aliased. For example if the FOV is 30 cm then

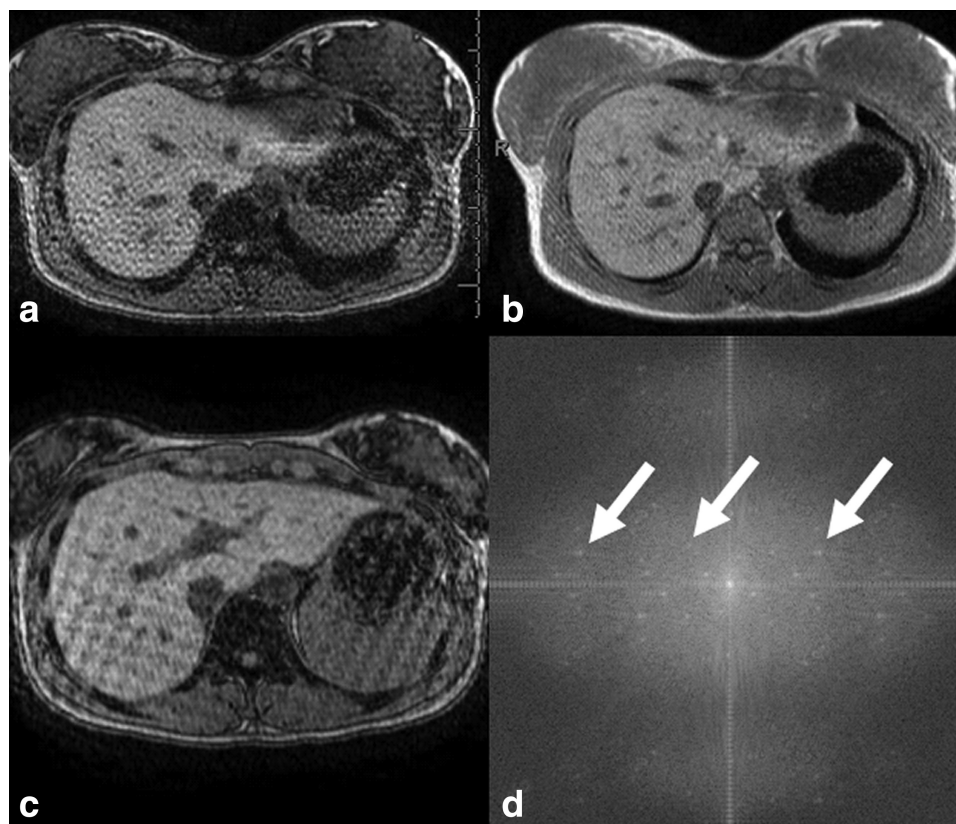


Figure 10. Spike noise artifacts. First (a) and second (b) echo images from 2D multislice dual gradient echo images (TEs 2.3 and 4.6 ms) demonstrating a cross-hatching artifact due to spike noise corrupting the raw data. Note that artifact is different at each echo time, as spikes occurred independently during each echo acquisition. c: Section slightly superior to a and b, note severe cross-hatching artifact. d: Fourier transform of c, showing a multitude of spikes (three of which are arrowed) accounting for the artifact.

tissue at 32 cm will appear at 2 cm, i.e., it will appear on the other side of the image.

Usually, phase aliasing is easy to recognize, but the resulting image can be confusing if the aliased body part is completely outside the FOV so that continuity from one side of the image to the other is difficult to recognize. Examples include an arm or hand mimicking a lesion, or enhancing vessels in the mediastinum resembling an enhancing tumor in the breast. Figure 11a shows a wrist aliased over the pelvis. A separate scan with a larger FOV (Fig. 11b) shows the wrist in its correct position. Simply swapping the phase and frequency directions, so that all the tissue along the phase axis is within the FOV, may be sufficient to eliminate these artifacts. However, if there are good reasons to place the direction of the phase encoding axis along the long axis of the patient, e.g. to control the direction of motion artifacts (see “Motion” below), or if both axes extend beyond the desired FOV, then it may be necessary to use no-phase-wrap techniques. These methods extend the original FOV in the phase encode direction, commonly by a factor of two, while commensurately reducing the number of signal averages to maintain the pixel size and signal-to-noise ratio. Tissue signal outside of the extended FOV aliases into the regions of extended FOV and are discarded resulting in the original FOV image being displayed but without any aliasing artifact. However,

if the body part is sufficiently large, aliasing may still degrade an image.

With 3D Fourier transform acquisitions, a second orthogonal phase encoding gradient is used to encode slices. Even though the excitation is often slab selective the profile of the excitation slab is not sharp at the edges, which means that some signal will be excited outside the range of the slice axis phase encoding. Therefore, data can be aliased in this direction as well as the axis of in-plane phase encoding. Because the aliased structures are at a level distant from the reconstructed image, this form of phase aliasing can be more confusing to understand. Viewing the top and bottom slices can usually clarify this artifact. The severity of slice axis phase aliasing can be reduced by using a receive coil of appropriate size, and positioning it properly. Figure 11c shows an image through the liver in which data from the right kidney, which is in the periphery of the axial excitation volume (Fig. 11d), are aliased into the image. Figure 11e shows that the coil was positioned too low, accentuating the aliasing.

Parallel Imaging

Parallel imaging comprises several methods that use the spatial information from multiple receiver coils to reduce acquisition times. There are two main classes

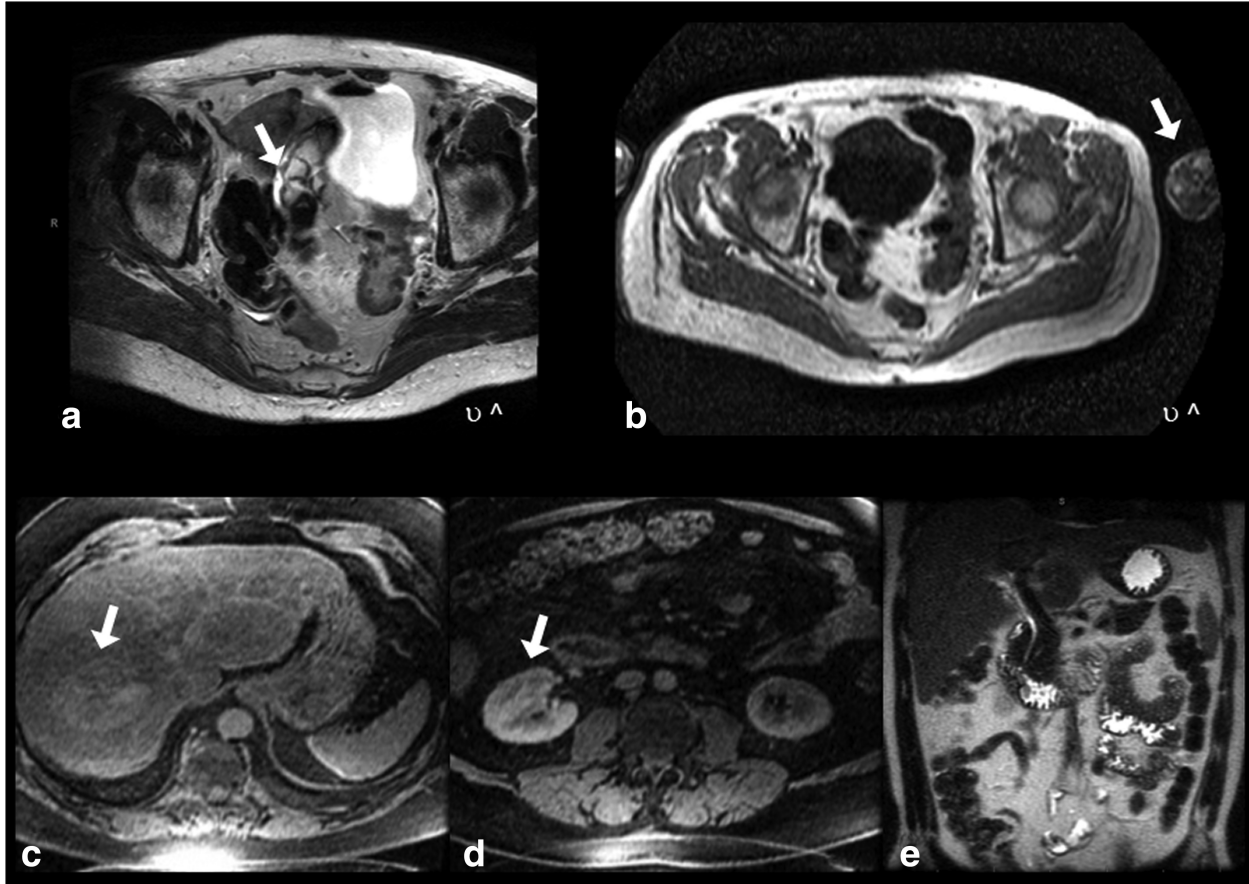


Figure 11. Examples of 2D and 3D phase encode aliasing artifacts. **a:** The FOV in the phase encoding direction is too small so that the left wrist (arrow) is aliased over the pelvis. **b:** The same acquisition with a larger field of view, shows the left wrist (arrow) in its correct location. **c,d:** Show 3D slab selection phase aliasing artifact. **c:** Axial image acquired using a 3D gradient echo technique shows a structure that appears to be within the liver (arrow). **d:** Image from the bottom slice of the acquisition in **c**, shows that the structure overlying the liver was aliasing from the right kidney (arrow). Note that **c** has higher SNR than **d**. **e:** The coronal single shot fast spin echo image illustrates the coil positioning used for **c** and **d**; note that signal intensity of the upper abdomen is lower than that of the lower abdomen. The coil was positioned too low, accentuating the aliasing of the right kidney into the liver. ν shows the frequency encoding direction. **c** and **d** are reproduced with permission from Yang RK, Roth CG, Ward RJ, et al. Optimizing abdominal MR imaging: approaches to common problems. *Radiographics* 2010;30:185-199.

of parallel imaging methods, those that work in the raw data or k -space domain and those that work in the image domain. The most common k -space-based techniques are Generalized Autocalibrating Partially Parallel Acquisitions (GRAPPA) (44) and Autocalibrating Reconstruction for Cartesian (ARC) imaging (45), whereas SENSitivity Encoding (SENSE) (46) is the most common image-based method. Both techniques derive their speed advantage by subsampling k -space such that a reduced number of phase encode steps are acquired. If the overall extent of k -space is unchanged but there is a greater spacing between phase encoding steps, image resolution is maintained but the phase FOV is reduced. As described above, reducing the phase FOV can result in phase aliasing or wrap. In k -space-based parallel imaging techniques, the coil sensitivity information is used to synthesize the missing lines of k -space so that the resultant images are free from aliasing, whereas in the image-based techniques, the coil sensitivity information is used to unwrap the images after reconstruction. One typical artifact that is often seen with

SENSE type reconstruction is shown in Figure 12a, where phase aliasing was present in the image before parallel imaging was applied (47). In a standard, i.e., nonparallel, imaging acquisition a small amount of wrap-around at the edges of an image, due to a reduced phase FOV, can often be tolerated (Fig. 12b). However, in the case of a SENSE-based acquisition and reconstruction such phase aliasing appears in the center of the image and may often cause problems in diagnosis, particularly if the artifact is subtle. For this reason, it is especially important to prescribe a large enough phase FOV, to accommodate the anatomy being imaged, whenever SENSE is used.

As described above SENSE parallel imaging implementations require knowledge of the individual coil spatial sensitivities to unwrap the image. These sensitivity maps are generally obtained before image acquisition as part of a calibration acquisition. There is, therefore, an assumption that the coil sensitivity profile does not change between acquisition of the calibration data and the image. However, if the patient or the coils move, the calibration may be suboptimal and incomplete

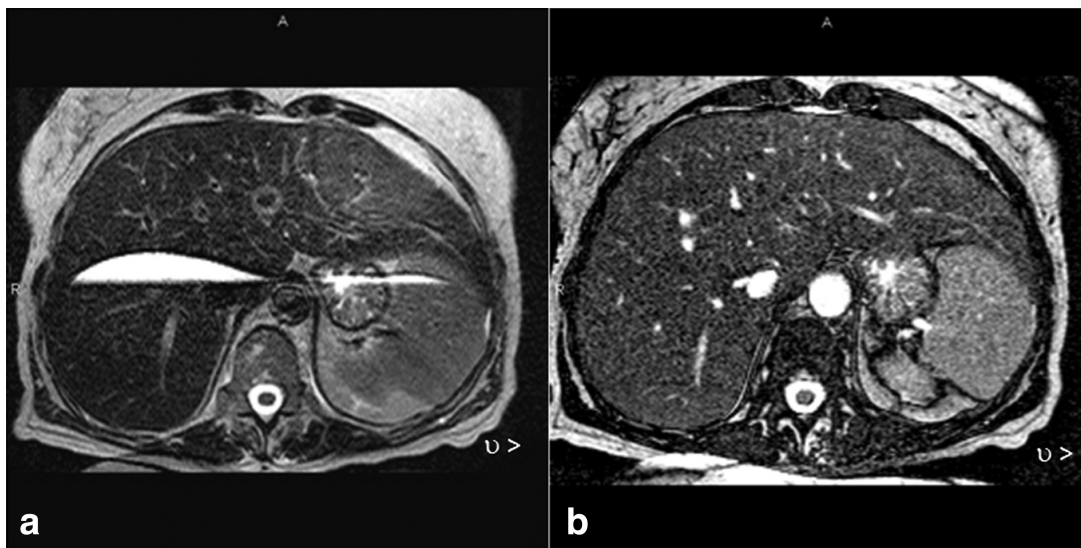


Figure 12. SENSE-based parallel imaging artifact. **a:** Single shot fast spin echo image obtained using image-based parallel imaging (SENSE) along the anteroposterior axis. Note the artifact in the center of the image due to the presence of image aliasing before acceleration. **b:** Balanced steady state free precession image at the same slice location as **a**, with same field of view but without SENSE. Note that the aliasing from the anterior abdominal wall now projects over the posterior portion of the image, where it is less problematic.

unwrapping may occur, even if the field FOV is large enough. In situations such as these, it may be necessary to repeat the calibration acquisition (Fig. 13).

Chemical Shift Effects

Because MRI uses magnetic field gradients to spatially localize signals based on their precessional frequency, the natural difference in frequency between the protons in water and fat means that they will appear spatially shifted in the frequency encoding direction (48,49). The amount of shift will depend upon the receiver bandwidth per pixel and the chemical shift at

the given field strength. A typical receiver bandwidth of ± 16 kHz over 256 pixels in the frequency encoding direction is equivalent to $\frac{32000}{256} = 125\text{Hz/pixel}$. At 1.5T the chemical shift induced frequency offset is approximately 220 Hz (see “Chemical Shift Selective Fat Saturation” above), so water and fat will be spatially shifted by $\frac{220}{125} = 1.76\text{pixels}$. Reducing the receiver bandwidth will increase the chemical shift offset and vice versa. Note that moving from 1.5T to 3.0T will double the offset for a given bandwidth. Figures 14a and b demonstrate chemical shift misregistration effects in two acquisitions acquired with two different receiver bandwidths.

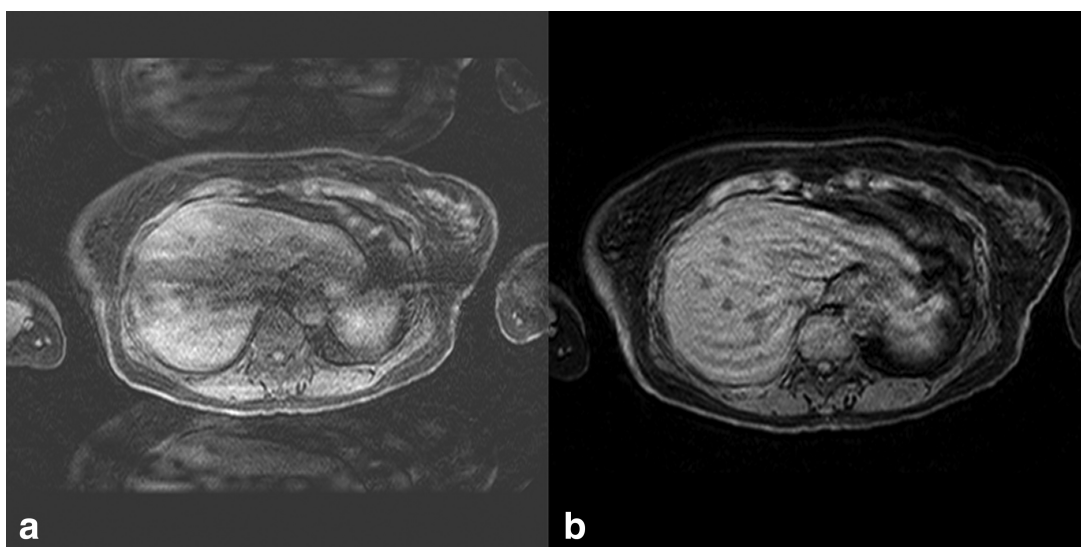


Figure 13. Parallel imaging miscalibration artifact. **a:** Axial 3D gradient echo image, using SENSE in the anteroposterior direction. There are severe coherent ghost artifacts anteriorly and posteriorly, different from the artifacts that would result from motion. Note that the edges of the liver and body wall are sharp, and that there is no visible motion-induced ghost artifact. **b:** As in **a**, but after repeating the SENSE calibration. The SENSE ghost artifacts are no longer present. Banding artifact at the edges of the liver may be a combination of motion and truncation artifacts.

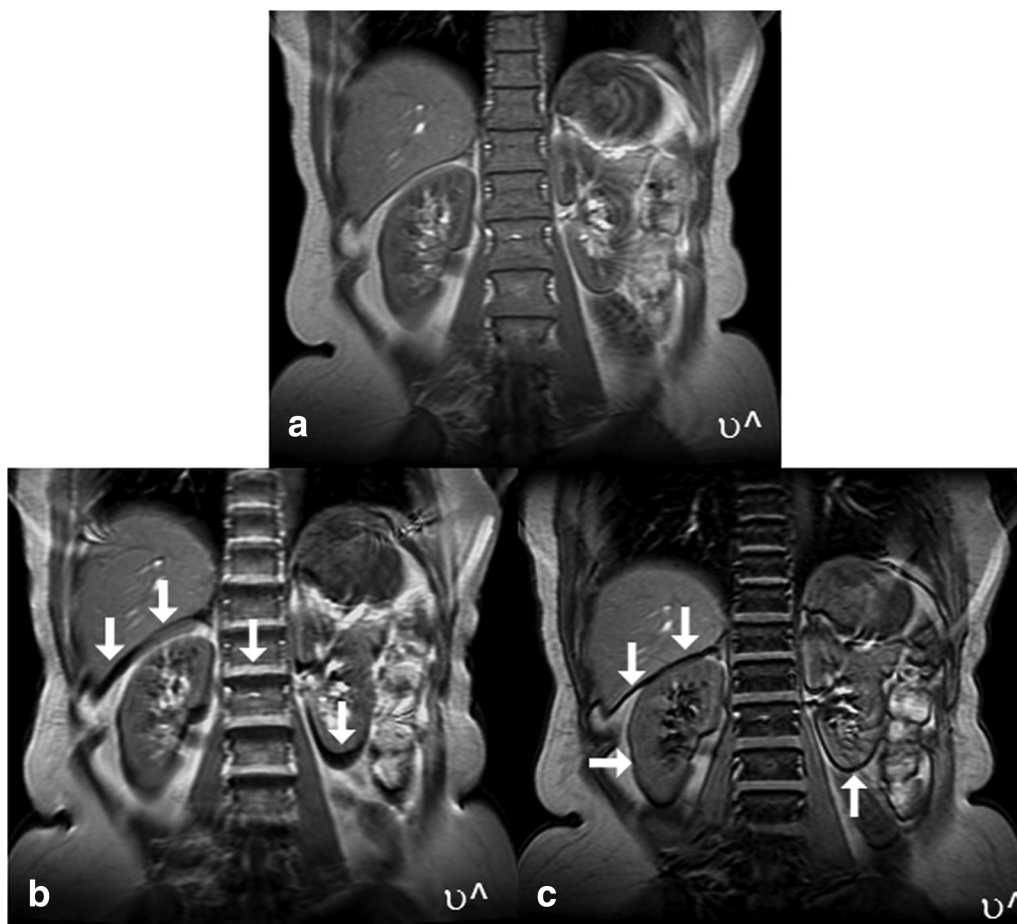


Figure 14. Chemical shift artifacts at 1.5T. **a:** Gradient echo image obtained with a receiver bandwidth of ± 62.5 kHz and an in-phase TE of 4.6 ms. **b:** Similar acquisition as in a but acquired with a receiver bandwidth of ± 7.82 kHz. Note the large chemical shift of 3.6 pixels in the frequency encoding direction (arrows) compared with 0.5 pixels in a. **c:** Similar acquisition as in a but obtained with an out-of-phase TE of 2.3 ms. Note the signal cancellation effects in those voxels containing an admixture of water and fat (arrows) compared with a. $\nu^$ shows the frequency encoding direction.

The frequency difference between water and fat of 220 Hz at 1.5T means that these signals are in-phase every time the relative phase evolves by an integral number of cycles. This corresponds to TEs at multiples of 4.6ms, i.e., 4.6 ms, 9.2 ms, etc (50). Conversely, they are in opposed-phase at the intermediate values 2.3 ms, 6.9 ms, etc. The result of using a TE where water and fat are out-of-phase is a signal cancellation effect in any voxels that contain both water and fat (Fig. 14c). Although chemical shift cancellation may be considered an image acquisition artifact, its observation is clinically useful for identifying lipid-containing tissues, which should have a signal reduction on out-of-phase imaging compared with in-phase imaging (51). This effect is also used in water/fat separation techniques (see “Water/Fat Separation” above). Note that the in- and out-of-phase appearance only applies to gradient echo imaging because the refocusing pulse in a spin echo acquisition cancels this phase shift, unless the echo is shifted from the position of perfect refocusing as implemented in Dixon’s original method (12).

Echo Train Blurring

Echo train techniques such as fast or turbo spin echo (FSE/TSE) sequences acquire multiple phase encodings following each excitation, within a single TR. A FSE/TSE sequence comprises a single excitation pulse (90°) followed by a train of refocusing pulses. Each refocusing pulse creates a spin echo and the phase encoding gradients are arranged such that each spin echo signal has a different phase encoding and can, therefore, be used in the same image k -space, which reduces the overall acquisition time. The operator-defined effective echo time (TE_{eff}) of the sequence dictates which of the multiple echoes has the smallest phase encoding gradient applied and, therefore, primarily affects the image contrast. A consequence of echo train imaging is that each of the echoes also undergoes T_2 decay during the acquisition. After Fourier transformation, the effect of this k -space signal decay is to cause blurring along the phase encoding direction, i.e., some of the signal from a single pixel will appear in adjacent pixels (52). For an exponentially decaying signal, the blurring can

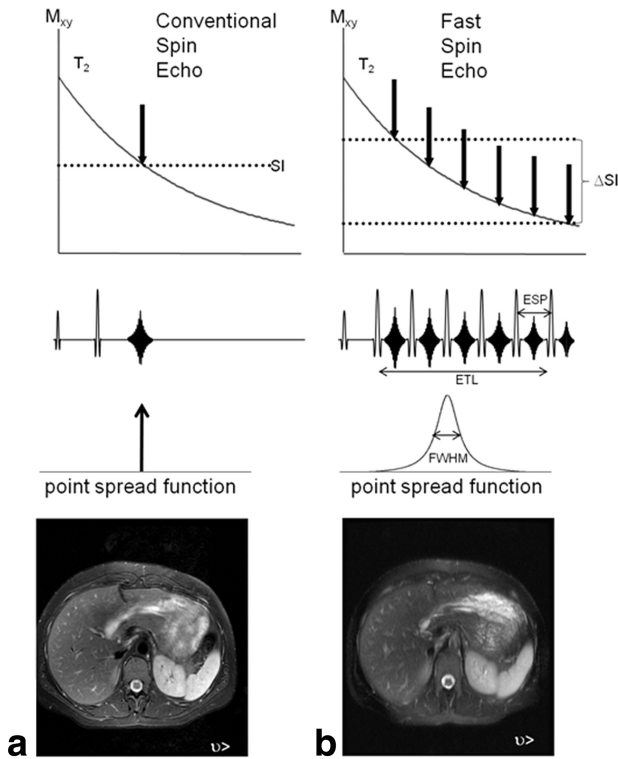


Figure 15. Blurring artifact in fast spin echo. **a:** Conventional spin echo (CSE) only acquires one phase encoding step per TR. Each echo has the same signal intensity (SI) which results in a singular point spread function (PSF) and a nonblurred image. **b:** Fast spin echo (FSE) acquires multiple phase encoding steps per TR. The diagram shows an echo train length (ETL) of 6; however, the image was acquired with an ETL of 32. Because each echo signal decreases due to T_2 relaxation each pixel has a broadened point spread function (PSF) resulting in a blurred image in the phase encode direction. Note that the CSF in the spinal cord which has a long T_2 demonstrates sharper margins. v shows the frequency encoding direction.

be represented as a Lorentzian point spread function (PSF). The degree of blurring can be estimated, by the full-width-at-half-maximum (FWHM) of the PSF and is given by:

$$FWHM = \frac{2 \cdot \Delta y \cdot ETL \cdot ESP}{\pi \cdot T_2} \quad [2]$$

Where Δy is the nominal pixel size in the phase encoding direction, ETL is the echo train length, and ESP is the echo spacing. Therefore, for a nominal 1 mm pixel size a tissue with a T_2 of 60 ms acquired with an ETL of 32 and an ESP of 5 ms will have a FWHM of 1.69 mm, i.e., the image will appear blurred in the phase encode direction compared with the nominal resolution. Tissues with short T_2 show substantial blur, while the long T_2 of simple fluid causes it to have little or no blur. Figure 15 demonstrates how data acquired over an echo train in FSE result in image blurring compared with a single echo conventional spin echo acquisition. Note that although most of the image in Figure 15b is blurry compared with

Figure 15a, the CSF in the spinal cord has sharper margins due to its longer T_2 . It should be noted that, in practice, the true k -space signal modulation and consequent PSF is dependent upon the phase encode ordering used and in particular, when the center of k -space is sampled with respect to the other spatial frequencies.

Motion

The MRI acquisition process assumes that the underlying tissue does not change in location or signal intensity during the acquisition. Any changes can cause modulation of the MRI signal, creating artifacts (53,54). Because a single frequency encoding is very rapid, motion does not generally cause artifacts in the frequency encoding direction. However, the interval between phase encoding steps in a conventional sequence, i.e., every TR, is more temporally commensurate with the rates of physiological motion. Hence, motion artifacts, regardless of the direction of the motion, will manifest as artifacts in the phase encoding direction, usually as “ghosting” whereby replicates of the moving structure are propagated along the phase encoding direction. Any type of movement can give rise to such ghosting appearances, including whole body motion, respiration, cardiac motion and blood flow. Many artifact reduction strategies focus on removing the motion (e.g., breath-holding), compensating for the motion (e.g., ECG-triggering, respiratory triggering or reordering phase encoding), suppressing the signal of moving tissue (e.g., spatial saturation (55)), signal averaging (56) or by using rapid imaging techniques. In some situations it may be possible to swap the phase and frequency directions (see “Phase Aliasing” above) to change the direction of the artifact and stop it from overlying a particular area of interest.

Figure 16 shows an example of ghosting due to respiratory motion. Anterior–posterior motion of the chest wall (in-plane) as well as inferior–superior motion of the liver (through-plane) causes a modulation of the MRI signal amplitude with time. After Fourier transformation, this modulated signal results in “sidebands” or ghosts, with the spacing of the ghosts proportional to the periodicity of the motion and inversely proportion to the TR (Fig. 16a). These sidebands appear as ghosts in the reconstructed image (Fig. 16b). Note that, with the use of surface coil arrays, the signal from subcutaneous fat is very high and exacerbates the appearance of the ghosts. In Figure 16c, the acquisition is respiratory-triggered so that data are only collected while the tissue is relatively stationary. Because there is no amplitude modulation there are no sidebands or ghosts appearing after reconstruction (Fig. 16d).

Similar amplitude modulation artifacts result from pulsatile flow in a vessel (57). Although the vessel itself is not moving, the changing signal intensity with differential flow-related signal enhancement throughout the cardiac cycle result in ghosting artifacts. It should also be noted that any system

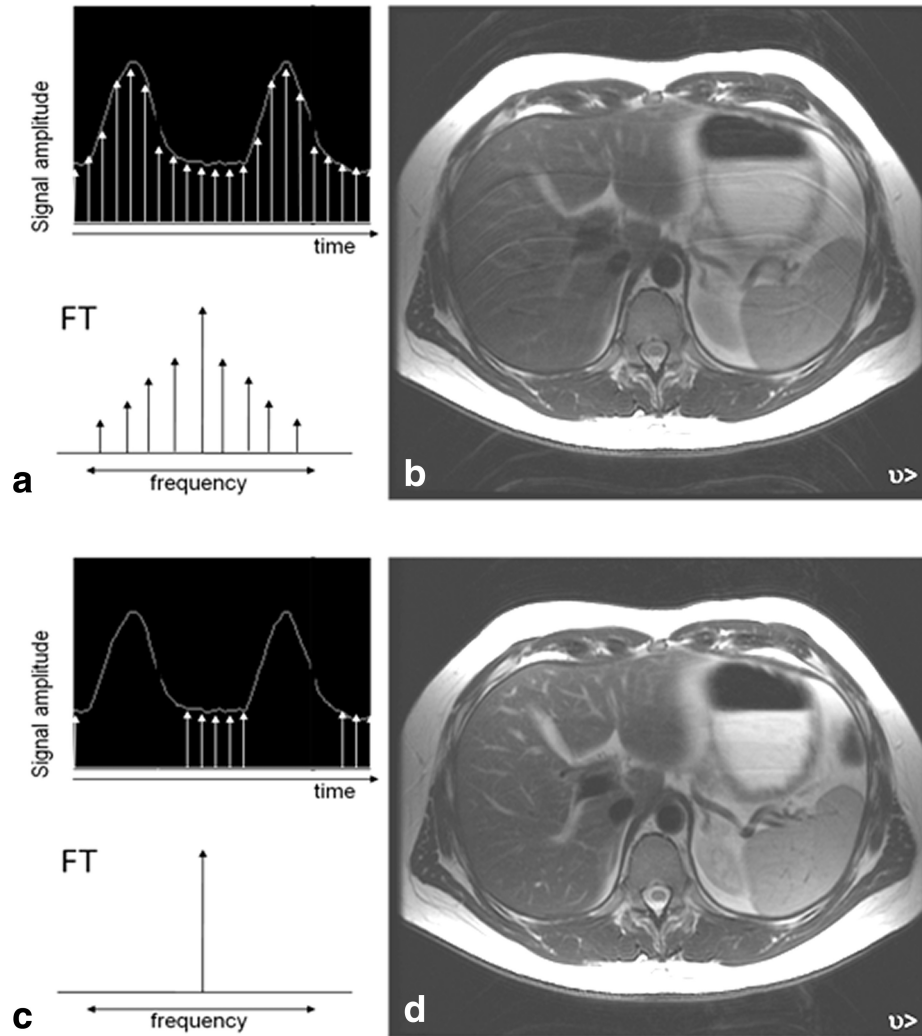


Figure 16. Respiratory motion artifact. **a:** Sampling data during the respiratory cycle cause an amplitude modulation of the MRI signal. Following Fourier transformation this amplitude modulation results in sidebands, which appear as ghosts in **b**. **c:** The use of respiratory triggering eliminates the amplitude modulation and the image exhibits minimal ghosting artifacts **d**. v shows the frequency encoding direction.

hardware instabilities can also cause signal modulation and hence ghosting in images.

Another category of motion induced artifact that can cause signal loss and ghosting arises from the phase shifts accumulated by spins moving during the application of the imaging gradients (58). This category of motion artifact can be greatly reduced by using gradient moment nulling techniques, called flow-compensation by some vendors, which involves using more complex gradient waveforms, usually on the slice select and frequency encoding axes, so that the phase accumulated by moving spins is zero, or nulled, at the end of the gradient waveform (59,60). The simplest form of gradient moment nulling involves correcting the phase shift due to spins moving with a constant velocity, known as the first order moment, which is the largest source of phase errors. Compensating for higher orders of motion, such as acceleration or jerk, requires more complex and longer duration gradient waveforms, meaning that they may cause more problems than they address. It

should be noted that even complete correction of gradient moment errors does not affect amplitude modulation, so that ghosting is still likely from pulsatile flow.

Some forms of motion artifact result from changes in tissue position that do not necessarily interfere with the process of phase encoding, and, therefore, do not produce ghost artifact along the phase encoding axis. As with any method of imaging, including conventional radiography, motion during image acquisition can produce artifacts. For example, image blurring or complex signal may occur when tissue occupies various positions during the period of image acquisition. Figure 17 shows an example where the changing shape of a vessel during image acquisition results in an image that suggests a filling defect.

One common motion-induced artifact results when images are calculated by subtracting one image from another, if the images are not perfectly registered. Subtraction images can be helpful to identify abnormal enhancement of a structure, but it is critical to

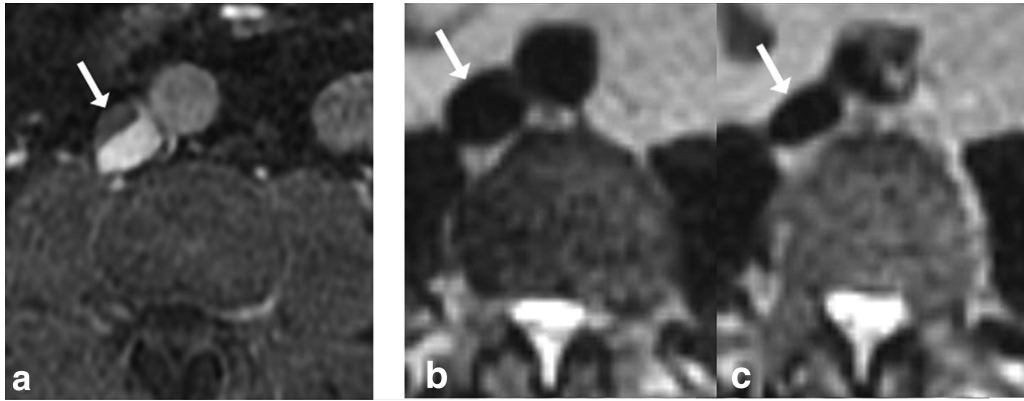


Figure 17. Artifact resembling thrombus within the IVC, caused by pulsatile changing shape of the IVC during the acquisition. **a:** Axial image from a 3D-gradient echo acquisition shows reduced signal in the anterior portion of the IVC suggesting thrombus (arrow). **b,c:** Adjacent single shot fast spin echo images showing varying size of IVC (arrows) due to pulsation, accounting for reduced signal at anterior portion of IVC in **a**. Note that **c** corresponds to the diastolic phase in the aorta, with collapse of the lumen compared with the lumen size shown in **b**. The smaller size of the lumen during diastole results in a region of low signal intensity within the anterior portion of the IVC lumen in **a**, mimicking thrombus.

avoid misdiagnosis due to spatial misregistration artifact (Fig. 18).

Subsecond imaging can reduce artifacts from periodic motion that cause ghosting and blurring, but changing intensity due to flow effects can produce inconsistent signal with ascites (Fig. 19) or large fluid collections. Additionally, the different flow velocities that occur in different portions of the cardiac cycle can cause inconsistent signal within the same vessel on adjacent image slices.

CONCLUSION

We hope that this review and the accompanying examples have been helpful to MRI clinicians who

help establish MR imaging protocols and interpret images, as well as to MRI physicists who are involved in helping clinicians with their tasks or designing and improving the performance of MRI systems. We trust that system interfaces can be improved and matched to MRI technologist training so that an MRI system's potential can more closely be realized. Radiologists, as well as anyone else who may be responsible for interpreting MR images, must improve their ability to recognize and understand artifacts so that they do not lead to diagnostic errors. Furthermore, understanding the nature and source of MRI artifacts can lead an informed radiologist to modify MR imaging protocols and instructions to MRI technologists so that artifacts and associated errors can be avoided in the future.

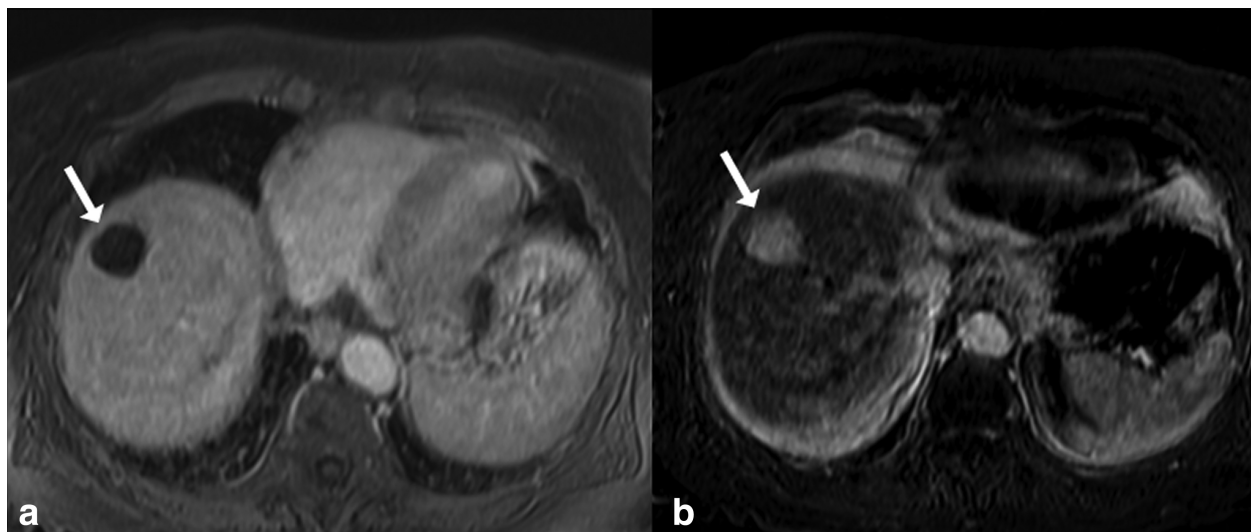


Figure 18. Subtraction artifact. **a:** Axial T1-weighted gradient echo image obtained three minutes after injection of a gadolinium contrast agent shows no enhancement of simple hepatic cyst (arrow). **b:** Image calculated by subtracting from **a** the unenhanced image (not shown) acquired at the identical location but in a separate breath-hold. Due to inconsistent breath-holding, the liver was present at the location of the cyst, creating an artifactual appearance of an enhancing liver lesion. The presence of mis-registration artifact can be determined by noticing the artifact at the edges of the liver.

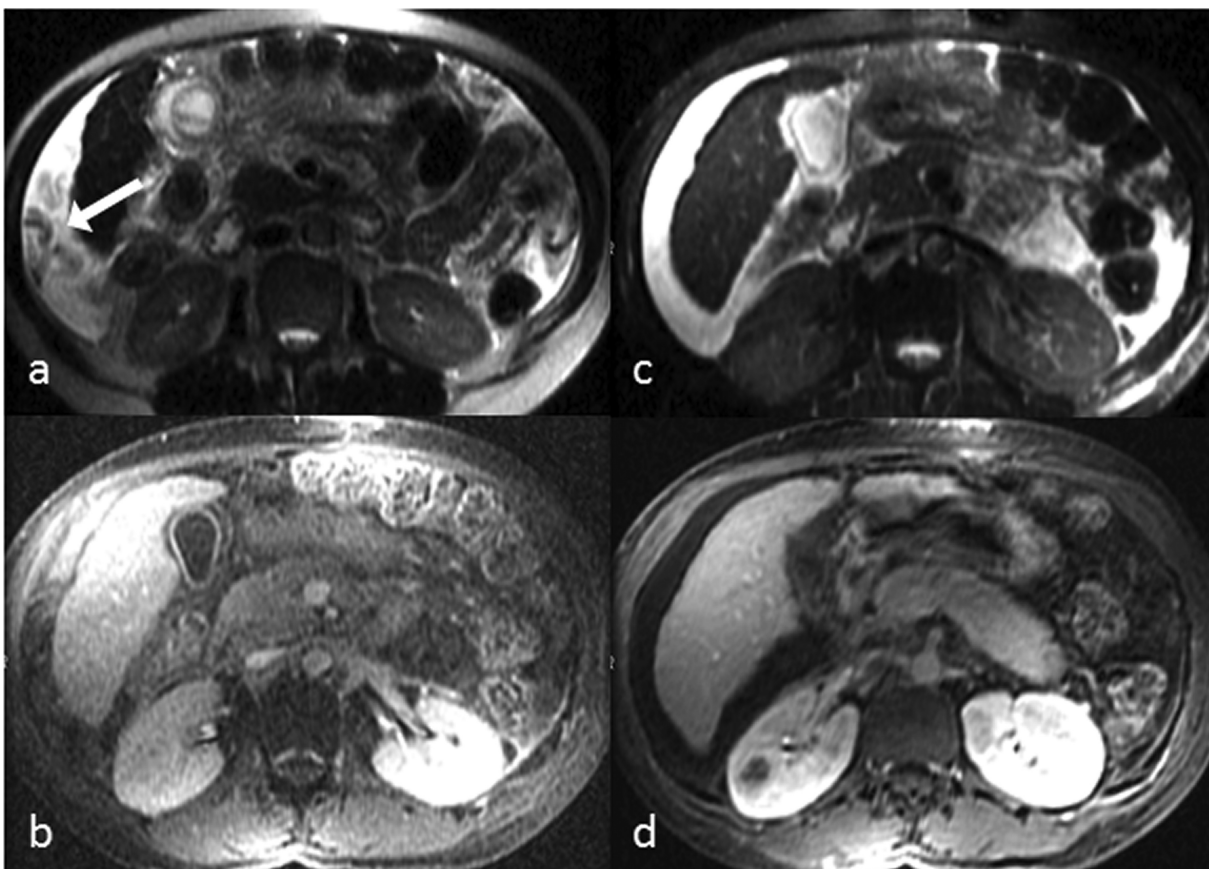


Figure 19. Fluid motion in ascites. **a:** Axial single slice fast spin echo image shows heterogeneous signal in ascites lateral to the inferior edge of the liver (arrow), due to motion of the fluid. **b:** Axial single slice gradient echo image, TR = 20 ms with acquisition time of 1 s, shows effects similar to those in **a**. **c:** Axial image acquired using a 2D multislice fast spin echo, where several slices were acquired during a 20-s suspended respiration. Averaging of motion during image acquisition has resulted in homogeneous signal of ascites. **d:** Axial image using 3D gradient echo technique, acquired during a 20-s suspended respiration, as in **c**, the ascites has homogeneous signal intensity.

ACKNOWLEDGMENTS

The authors thank Dr. Christopher J. Hardy and Dr. Ferdia Gallagher for helpful discussions.

REFERENCES

- Bellon EM, Haacke EM, Coleman PE, Sacco DC, Steiger DA, Gangarosa RE. MR artifacts: a review. *AJR Am J Roentgenol* 1986;147:1271-1281.
- Mirowitz SA. MR imaging artifacts. Challenges and solutions. *Magn Reson Imaging Clin N Am* 1999;7:717-732.
- Bernstein MA, Huston J III, Ward HA. Imaging artifacts at 3.0T. *J Magn Reson Imaging* 2006;24:735-746.
- Zhuo J, Gullapalli RP. AAPM/RSNA physics tutorial for residents: MR artifacts, safety, and quality control. *Radiographics* 2006;26:275-297.
- Stadler A, Schima W, Ba-Ssalamah A, Kettenbach J, Eisenhuber E. Artifacts in body MR imaging: their appearance and how to eliminate them. *Eur Radiol* 2007;17:1242-1255.
- Morelli JN, Runge VM, Ai F, et al. An image-based approach to understanding the physics of MR artifacts. *Radiographics* 2011;31:849-866.
- Schneider E, Glover G. Rapid in vivo proton shimming. *Magn Reson Med* 1991;18:335-347.
- Yoshimitsu K, Varma DG, Jackson EF. Unsuppressed fat in the right anterior diaphragmatic region on fat-suppressed T2-weighted fast spin-echo MR images. *J Magn Reson Imaging* 1995;5:145-149.
- Axel L, Kolman L, Charafeddine R, Hwang SN, Stolpen AH. Origin of a signal intensity loss artifact in fat-saturation MR imaging. *Radiology* 2000;217:911-915.
- Anzai Y, Lufkin RB, Jabour BA, Hanafee WN. Fat-suppression failure artifacts simulating pathology on frequency-selective fat-suppression MR images of the head and neck. *AJNR Am J Neuro-radiol* 1992;13:879-884.
- Siegelman ES, Charafeddine R, Stolpen AH, Axel L. Suppression of intravascular signal on fat-saturated contrast-enhanced thoracic MR arteriograms. *Radiology* 2000;217:115-118.
- Dixon WT. Simple proton spectroscopic imaging. *Radiology* 1984;153:189-194.
- Ma J. Breath-hold water and fat imaging using a dual-echo two-point Dixon technique with an efficient and robust phase-correction algorithm. *Magn Reson Med* 2004;52:415-419.
- Reeder SB, Pineda AR, Wen Z, et al. Iterative decomposition of water and fat with echo asymmetry and least-squares estimation (IDEAL): application with fast spin-echo imaging. *Magn Reson Med* 2005;54:636-644.
- Rosenfeld D, Panfil SL, Zur Y. Design of adiabatic pulses for fat-suppression using analytic solutions of the Bloch equation. *Magn Reson Med* 1997;37:793-801.
- Hargreaves BA. Rapid gradient-echo imaging. *J Magn Reson Imaging* 2012;36:1300-1313.
- Zur Y, Stokar S, Bendel P. An analysis of fast imaging sequences with steady-state transverse magnetization refocusing. *Magn Reson Med* 1988;6:175-193.
- Kolind SH, MacKay AL, Munk PL, Xiang QS. Quantitative evaluation of metal artifact reduction techniques. *J Magn Reson Imaging* 2004;20:487-495.

19. Mansfield P, Chapman BLW. Active magnetic screening of gradient coils in NMR imaging. *J Magn Reson* 1986;66:573–576.
20. Roemer PB, Hickey JS. Self-shielded gradient coils for nuclear magnetic resonance imaging. US Patent 1988; 4,737,716.
21. Morich MA, Lapman DA, Lannels WR, Goldie FT. Exact temporal eddy current compensation in magnetic resonance imaging systems. *IEEE Trans Med Imaging* 1988;7.
22. Van Vaals JJ, Bergman AH. Optimization of eddy current compensation. *J Magn Reson* 1990;90:52–70.
23. Walker PG, Cranney GB, Scheidegger MB, Waseleski G, Pohost GM, Yoganathan AP. Semiautomated method for noise reduction and background phase error correction in MR phase velocity data. *J Magn Reson Imaging* 1993;3:521–530.
24. Lingamneni A, Hardy PA, Powell KA, Pelc NJ, White RD. Validation of cine phase-contrast MR imaging for motion analysis. *J Magn Reson Imaging* 1995;5:331–338.
25. Hinks RS. Fast spin echo prescan for MRI system. U.S. Patent 1995; 5,378,985.
26. Ma J, Zhou X. Fast spin echo phase correction for MRI system. U.S. Patent 2002; 6,369,568.
27. Glover GH, Pelc NJ. Method for correcting image distortion due to gradient nonuniformity. U.S. Patent 1986; 4,591,789.
28. Doran SJ, Charles-Edwards L, Reinsberg SA, Leach MO. A complete distortion correction for MR images: I. Gradient warp correction. *Phys Med Biol* 2005;50:1343–1361.
29. Collins CM, Liu W, Schreiber W, Yang QX, Smith MB. Central brightening due to constructive interference with, without, and despite dielectric resonance. *J Magn Reson Imaging* 2005;21:192–196.
30. Sreenivas M, Lowry M, Gibbs P, Pickles M, Turnbull LW. A simple solution for reducing artifacts due to conductive and dielectric effects in clinical magnetic resonance imaging at 3T. *Eur J Radiol* 2007;62:143–146.
31. Franklin KM, Dale BM, Merkle EM. Improvement in B1-inhomogeneity artifacts in the abdomen at 3T MR imaging using a radiofrequency cushion. *J Magn Reson Imaging* 2008;27:1443–1447.
32. Barth MM, Smith MP, Pedrosa I, Lenkinski RE, Rofsky NM. Body MR imaging at 3.0 T: understanding the opportunities and challenges. *Radiographics* 2007;27:1445–1462; discussion 1462–1444.
33. Katscher U, Bornert P. Parallel RF transmission in MRI. *NMR Biomed* 2006;19:393–400.
34. Yarnykh VL. Actual flip-angle imaging in the pulsed steady state: a method for rapid three-dimensional mapping of the transmitted radiofrequency field. *Magn Reson Med* 2007;57:192–200.
35. Sacolick LI, Wiesinger F, Hancu I, Vogel MW. B1 mapping by Bloch-Siegert shift. *Magn Reson Med* 2010;63:1315–1322.
36. Roemer PB, Edelstein WA, Hayes CE, Souza SP, Mueller OM. The NMR phased array. *Magn Reson Med* 1990;16:192–225.
37. Vovk U, Pernus F, Likar B. A review of methods for correction of intensity inhomogeneity in MRI. *IEEE Trans Med Imaging* 2007; 26:405–421.
38. Steckner MC, Dannels WR. The FSE “cusp” artifact: interactions between rf rolloff, gradient rollover, and B0 homogeneity. In: Proceedings of the 3rd Annual Meeting of ISMRM, Nice, France, 1995. (abstract 756).
39. Kim JK, White LM, Hinks RS, King KF. The FSE cusp artifact: a phase wrap-in artifact seen on routine clinical MR images of the knee. In: Proceedings of the 7th Annual Meeting of ISMRM, Philadelphia, Pennsylvania, 1999. (abstract 1033).
40. King KF, Hinks RS. Method and system of MR imaging with reduced FSE cusp artifacts. U.S. Patent 2007; 7,250,762.
41. Frederick PS, Johnson JA. Method for reducing artifacts in MR images acquired with phased array surface coil. U.S. Patent 2000; 6,134,465.
42. Foo TF, Grigsby NS, Mitchell JD, Slayman BE. SNORE: spike noise removal and detection. *IEEE Trans Med Imaging* 1994;13:133–136.
43. Edelstein WA, Hutchison JM, Johnson G, Redpath T. Spin warp NMR imaging and applications to human whole-body imaging. *Phys Med Biol* 1980;25:751–756.
44. Griswold MA, Jakob PM, Heidemann RM, et al. Generalized autocalibrating partially parallel acquisitions (GRAPPA). *Magn Reson Med* 2002;47:1202–1210.
45. Brau AC, Beatty PJ, Skare S, Bammer R. Comparison of reconstruction accuracy and efficiency among autocalibrating data-driven parallel imaging methods. *Magn Reson Med* 2008;59:382–395.
46. Pruessmann KP, Weiger M, Scheidegger MB, Boesiger P. SENSE: sensitivity encoding for fast MRI. *Magn Reson Med* 1999;42:952–962.
47. Goldfarb JW. The SENSE ghost: field-of-view restrictions for SENSE imaging. *J Magn Reson Imaging* 2004;20:1046–1051.
48. Babcock EE, Brateman L, Weinreb JC, Horner SD, Nunnally RL. Edge artifacts in MR images: chemical shift effect. *J Comput Assist Tomogr* 1985;9:252–257.
49. Dwyer AJ, Knop RH, Hoult DI. Frequency shift artifacts in MR imaging. *J Comput Assist Tomogr* 1985;9:16–18.
50. Wehrli FW, Perkins TG, Shimakawa A, Roberts F. Chemical shift-induced amplitude modulations in images obtained with gradient refocusing. *Magn Reson Imaging* 1987;5:157–158.
51. Mitchell DG. Chemical shift magnetic resonance imaging: applications in the abdomen and pelvis. *Top Magn Reson Imaging* 1992;4:46–63.
52. Constable RT, Anderson AW, Zhong J, Gore JC. Factors influencing contrast in fast spin-echo MR imaging. *Magn Reson Imaging* 1992;10:497–511.
53. Wood ML, Henkelman RM. MR image artifacts from periodic motion. *Med Phys* 1985;12:143–151.
54. Barish MA, Jara H. Motion artifact control in body MR imaging. *Magn Reson Imaging Clin N Am* 1999;7:289–301.
55. Felmlee JP, Ehman RL. Spatial presaturation: a method for suppressing flow artifacts and improving depiction of vascular anatomy in MR imaging. *Radiology* 1987;164:559–564.
56. Gazelle GS, Saini S, Hahn PF, Goldberg MA, Halpern EF. MR imaging of the liver at 1.5 T: value of signal averaging in suppressing motion artifacts. *AJR Am J Roentgenol* 1994;163:335–337.
57. Perman WH, Moran PR, Moran RA, Bernstein MA. Artifacts from pulsatile flow in MR imaging. *J Comput Assist Tomogr* 1986;10:473–483.
58. van Dijk P. Direct cardiac NMR imaging of heart wall and blood flow velocity. *J Comput Assist Tomogr* 1984;8:429–436.
59. Haacke EM, Lenz GW. Improving MR image quality in the presence of motion by using rephasing gradients. *AJR Am J Roentgenol* 1987;148:1251–1258.
60. Ehman RL, Felmlee JP. Flow artifact reduction in MRI: a review of the roles of gradient moment nulling and spatial presaturation. *Magn Reson Med* 1990;14:293–307.